Transport Dynamics and Multi-Scale Coupling of Turbulence in LHD

Shigeru INAGAKI, Naoki TAMURA[1)], Yoshihiko NAGASHIMA, Tokihiko TOKUZAWA[1)], Takuma YAMADA, Katsumi IDA[1)], Takashi MARUTA[2)], Shin KUBO[1)], Kenichi TERASAKA[2)], Takashi SHIMOZUMA[1)], Yoshio NAGAYAMA[1)], Kazuo KAWAHATA[1)], Akio KOMORI[1)], Shunjiro SHINOHARA[2)], Akihide FUJISAWA[1)], Masatoshi YAGI, Yoshinobu KAWAI, Sanae-I. ITOH, Kimitaka ITOH[1)] and the LHD experimental group

RIAM, Kyushu University, 6-1 Kasuga-Koen, Kasuga 816-8580, Japan
[1)]*National Institute for Fusion Science,322-6 Oroshi-cho, Toki 509-5292, Japan*
[2)]*IGSES, Kyushu University, 6-1 Kasuga-Koen, Kasuga 816-8580, Japan*

(Received 16 November 2007 / Accepted 27 March 2008)

Spatiotemporal correlation of heat transport and micro- to meso- scale or macro-scale coupling of plasma turbulence are investigated in LHD plasmas, where fast propagation of a cold pulse and a non-local temperature rise are observed. Evidence of a timescale shorter than the diffusion time and a spatial scale longer than the micro-turbulence correlation length between core heat fluxes and edge temperature gradients is found. At the same time, an envelope of turbulent density fluctuations is also found to be modulated. Observation of low frequency ($\leq$ 2 kHz) amplitude modulation of density fluctuation suggests the existence of meso- to macro-scale turbulent structures in the plasma, in which a non-local temperature rise takes place. Relationships between the turbulence with long radial correlation length and the edge-core coupling of heat transport are discussed.

Keywords: non-local transport, fluctuation, reflectometry, LHD

DOI: 10.1585/pfr.3.S1006

1. Introduction

Turbulence transport is higher than the neoclassical level in helical devices (heliotron, stellarators, heliac, etc) as well as in tokamaks except for the transport barrier regions and the core region in the low density regime of medium size helical devices [1, 2]. In the paradigm of turbulence transport in toroidal plasmas, it is presumed that local turbulence led by a local microinstability drives local transport. In turbulent transport, the flux is predicted to be a non-linearly increasing function of the gradient. The radial correlation length of micro-turbulence is of the order of the ion gyro-radius and is hence usually much smaller than the temperature gradient scale length. Thereby, turbulence transport is considered to be a local process even if it is non-linear. Non-linear but local transport models have been proposed and tested. Such models can explain features of electron transport in stationary regimes. However, the transient plasma responses cannot be predicted. Fast propagation of a temperature perturbation has often been observed such as the ballistic propagation observed in TJ-II [3], heat pulse propagation caused by the L-H transition [4] and heating power switching [5]. These abrupt core responses are evident before diffusive transport effects reach the core region. In addition, the core temperature T_e often rises in response to edge cooling in many tokamaks and LHD [6–10]. These features of electron transport in transient regimes introduce a non-locality, which is a fundamental problem of the turbulent transport model. To understand elemental steps of turbulence transport, studies of spatiotemporal scale of transport phenomena are important. The timescales of non-local transport phenomena are compared to local diffusion time, however, the spatial scales have not been discussed quantitatively. Recent theoretical and simulation works on turbulence show that zonal flows driven by drift wave turbulence play an important role in saturating the level of turbulence, as well as turbulent transport [11–14]. Zonal flows can be considered as non-linear instability associated with multi-scale coupling of waves (inverse cascade of the turbulent spectra). To clarify the relationships between multi-scale coupling of turbulence and the features of turbulence transport, analyses of spatial scales of transport and turbulence correlation, as well as the timescales are important. In this paper, we report the radial correlation scale of non-local transport using the correlation function between the heat flux and temperature gradient at two different radii in the transient regimes on LHD. At the same time, multi-scale coupling of turbulence is observed with conventional reflectometry using a new analysis method.

author's e-mail: inagaki@riam.kyushu-u.ac.jp

2. Non-Local Transport in LHD

Some local transport models based on temperature-gradient-driven turbulence indicate that heat transport is non-linear, and thus, electron heat diffusivity, χ_e, has a dependence on T_e and/or ∇T_e [15]. To study the non-linearity of heat transport, transient experiments (inducing cold and/or heat pulses) have been performed [16]. Fast propagation of temperature perturbation was often observed, e.g. the ballistic propagation observed in TJ-II [3], heat pulse propagation caused by the L-H transition [4] and heating power switching [5]. If χ_e has a dependence like $\chi_e \propto \nabla T_e{}^{\alpha}$, $\alpha \sim 50$ is required to explain these transient responses. Fast propagation of a cold pulse tends to be observed in large tokamaks rather than small-to-medium size tokamaks. This tendency has not been confirmed in helical devices, but for a comprehensive understanding of transport non-locality, its presence or absence must be determined. Cold pulse experiments in LHD [17] are therefore crucial. Fast propagation is indeed observed in LHD as well as in large tokamaks. Figure 1 shows the typical time evolution of a cold pulse induced by tracer encapsulated solid pellet (TESPEL) injection in low density ($1 \times 10^{19}\mathrm{m}^{-3}$) NBI plasma to LHD (with a major radius at the magnetic axis of $R_{ax} = 3.5/3.6$ m, an averaged minor radius of $a = 0.6$ m and a magnetic field of up to 2.83T at axis) [18]. The T_e perturbation, δT_e, simulated using models with $\chi_e = \chi_{pb}$ and $\chi_e \propto \nabla T_e{}^{\alpha}$ are also shown, where χ_{pb} is the heat diffusivity determined using the power balance analysis in stationary state [19]. In the simulation, δT_e is calculated from the perturbation equation written as

$$\frac{3}{2} n_e \frac{\partial \delta T_e}{\partial t} = -\nabla \cdot \delta q_e \qquad (1)$$

by using a time dependent boundary condition. The simulation using the $\chi = \chi_{pb}$ model (blue lines in Fig. 1) demarcates the local diffusion effect. The core T_e begins to decrease before the diffusive transport effect reaches the core region. To explain this prompt response of the core T_e by the non-linearity of χ_e, a strong ∇T_e dependence of χ_e ($\alpha = 7$) is required (see red lines in Fig. 1). On the other hand, α = 1-3/2 (gyro-Bohm type T_e dependence on heat diffusivity) is required to explain the stationary transport property both in tokamaks and helical devices [19]. A new perspective to turbulence transport (i.e. non-locality) has been introduced to explain this discrepancy. Fast propagation is also observed in TJ-II. Non-local transport, therefore, may easily arise in helical devices due to differences in magnetic configuration (e.g., local and global magnetic shears).

In addition to fast propagation, core T_e often rises in response to edge cooling in many tokamaks and LHD [6–10]. A significant core T_e rise has been observed by TESPEL injection in LHD as shown in Fig. 2 (a) (for more

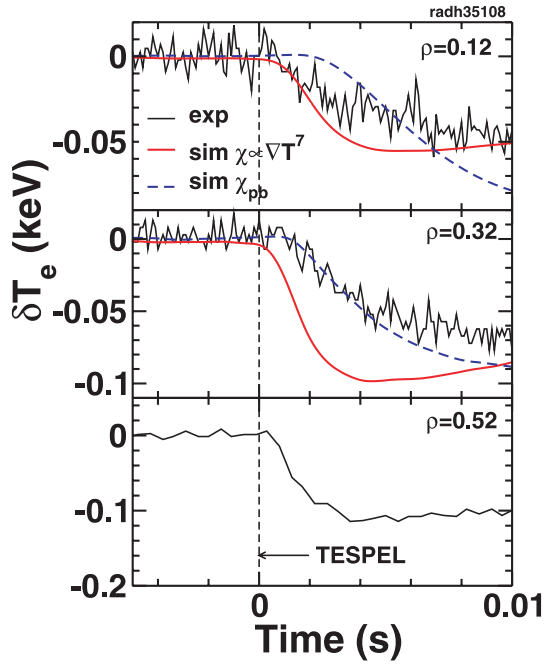

Fig. 1 Time evolution of δT_e at three different normalized radii. The simulation results based on models of $\chi_e = \chi_{pb}$ and $\chi_e \propto \nabla T_e{}^{\alpha}$, $\alpha = 7$ are also shown.

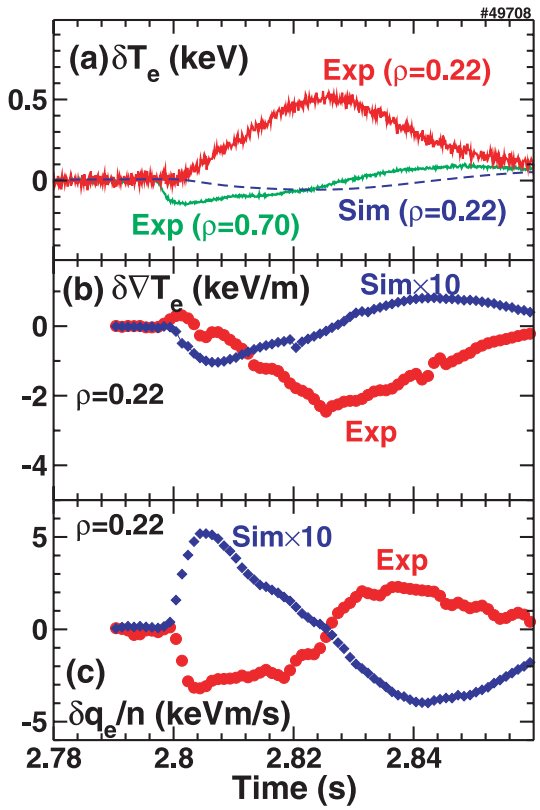

Fig. 2 Time evolution of (a) δT_e at two different normalized radii, (b) $\delta \nabla T_e$ at $\rho = 0.22$ and (c) δq_e at $\rho = 0.22$. Simulation result based on the power balance χ model are also shown (blue line or blue diamonds). The simulated results are much smaller than experimental observations, and are thus multiplied by ten in this figure.

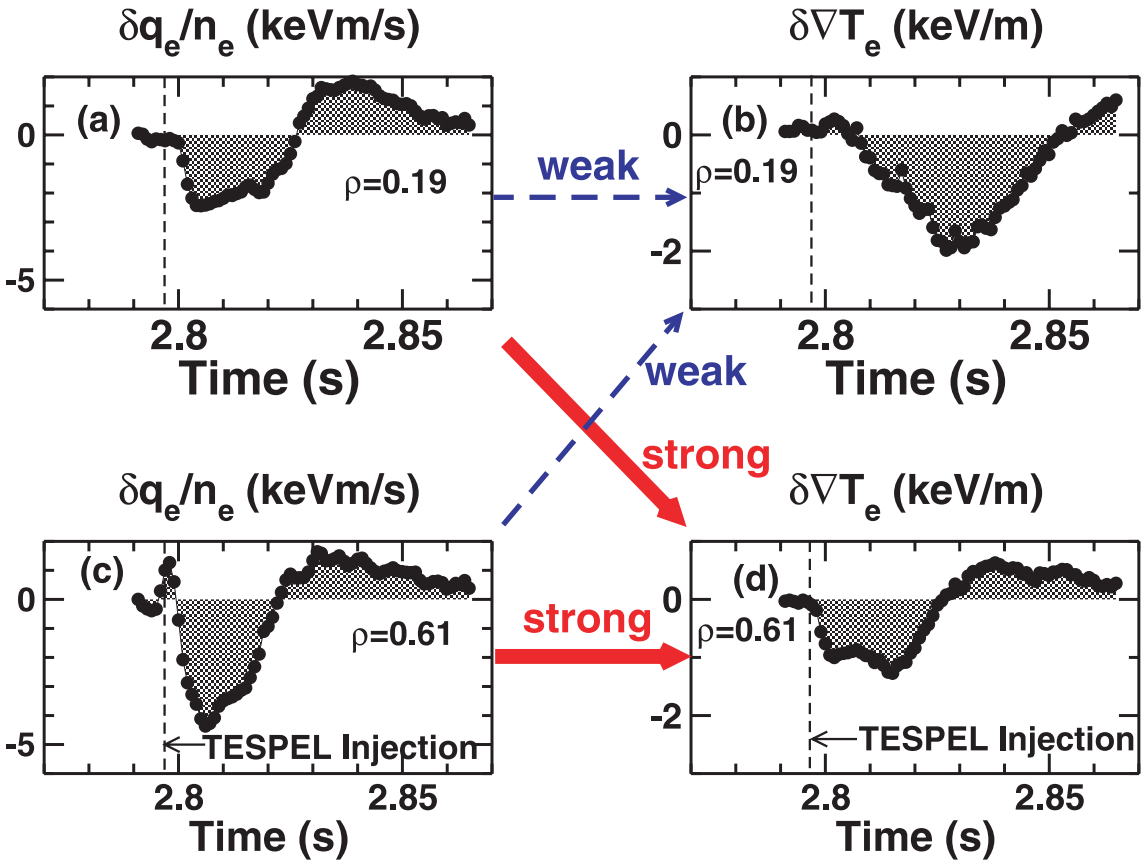

Fig. 3 Time evolution of the δq_e and the $\delta \nabla T_e$ at the core ($\rho = 0.19$) and the edge ($\rho = 0.61$).

details see ref. [9]). Typical parameters in this experiment are as follows: a line averaged density of 1-2 $\times 10^{19}$ m^{-3}, central electron temperature of $\geq$ 1.5 keV, central ion temperature of 1-2 keV, plasma β value of 0.1 %, absorbed ECH power of 0.8 MW, and deposited neutral beam power of 2 MW. Characteristic spatial and time scales are the ion Larmor radius $\rho_i \sim 1$ mm, $c/\omega_p \sim 2$ mm, typical spatial scale of meso-scale structure $\sqrt{a\rho_i} \sim 30$ mm, $a/c_s \sim 1$ µs, global energy confinement time of 50 ms and meso-scale time $\sqrt{(a/\rho_i)(a/c_s)} \sim 30$ µs, where ω_p is the plasma frequency, c is the speed of light and c_s is the ion sound velocity. The relationship between heat flux and temperature gradient is essential to understand heat transport. Thus, time evolutions of the core ∇T_e perturbation and heat flux perturbation (normalized by density) are also shown in Fig. 2 (b). A multi-channel heterodyne radiometer is used to track small T_e perturbations at different normalized radii [20]. The absolute error of ∇T_e determined by the absolute calibration of ECE is 20 % and the relative error of ∇T_e determined by the noise levels of ECE is only 1 %. The electron heat flux perturbation can be determined from the perturbation equation,

$$\delta q_e(\rho, t) = -\frac{1}{S(\rho)} \int_0^{\rho} \frac{3}{2} n_e \frac{\partial \delta T_e(\rho, t)}{\partial t} dV, \qquad (2)$$

where S is the surface area of the closed flux surface and V is the volume. The power balance simulation (blue diamonds in Fig. 2) indicates small changes in the temperature gradient and heat flux in the core region, which differ from the experimental observations (red diamonds in Fig. 2). In addition, the local transport assumption cannot explain the change of sign in the heat flux. In spite of the smooth change in the temperature gradient, abrupt reductions in the heat flux (heat flux jump) are observed after several ms from the TESPEL injection. The relationship between heat flux and ∇T_e is essential to discuss whether or not transport is local (diffusive). To survey local and non-local coupling, δq_e and $\delta \nabla T_e$ at the core ($\rho = 0.19$) and the edge ($\rho = 0.61$) are shown in Fig. 3. To determine the strength of coupling between the heat flux and temperature gradient, two-point cross-correlations between the core and edge are calculated. The cross-correlation is defined as

$$C_{f,g}(\rho_{ref}, \rho, \tau) = \frac{\langle f(\rho_{ref}, t) g(\rho, t+\tau) \rangle}{\sqrt{\langle f^2(\rho_{ref}, t) \rangle \langle g^2(\rho, t) \rangle}}, \qquad (3)$$

where $\langle\rangle$ denotes the temporal average, defined as $\langle h(t) \rangle = (T)^{-1} \int_0^T h(t) dt$. Due to the similarity of the figures, strong correlations between the core heat flux and edge temperature gradient and between the edge heat flux and edge temperature gradient are expected. On the other hand, weak correlations between the core heat flux and core temperature gradient and between edge heat flux and core temperature gradient are predicted. Figure 4 indicates the

cross-correlation functions, $C_{\delta q_e/n_e,-\delta\nabla T_e}(\rho_{\delta q_e/n_e},\rho_{\delta\nabla T_e},\tau)$, between core heat flux and core temperature gradient (local correlation: $\rho_{\delta q_e/n_e}=0.19$, $\rho_{\delta\nabla T_e}=0.19$), the core heat flux and edge temperature gradient (non-local correlation: $\rho_{\delta q_e/n_e}=0.19$, $\rho_{\delta\nabla T_e}=0.61$), and the edge heat flux and edge temperature gradient (local correlation: $\rho_{\delta q_e/n_e}=0.61$, $\rho_{\delta\nabla T_e}=0.61$). In the paradigm for local diffusion, a strong correlation between $q_e(\rho)$ and $\nabla T_e(\rho)$ is trivial and the relation $\delta q_e = -n_e\chi_{pb}\nabla\delta T_e$ is indeed satisfied in a simulation. The cross-correlation between the simulated core $\delta q_e/n_e$ and the simulated core $\delta\nabla T_e$ is strong at $\tau=0$ and decreases gradually as τ increses, as shown by the black dashed line in Fig. 4 (a). On the other hand, the experimentally obtained core-to-core correlation is weak (~ 0) at $\tau=0$ and increases gradually as τ increases and then decreases with a timescale similar to the simulation result for $\tau \geq 15$ ms. Moreover, the experimental result indicates that the core ($\rho=0.19$) heat flux is strongly coupled with the edge ($\rho=0.61$) temperature gradient for a short τ as shown in Fig. 4 (b), and therefore, the presence of a long distance/non-local correlation between heat flux and temperature gradient is clarified. The correlation length ($\sim a$) is obviously larger than the order of meso-scales (~ 30 mm) and thus global scales. The strong negative non-local correlation is reduced with an increase in τ on a timescale similar to the local transport. On the contrary, the edge heat flux is not coupled with the core temperature gradient. This may correspond to the experimental results that indicate that there is no non-local response in heat pulse propagation induced by ECH modulation in LHD. The local edge-to-edge correlation (Fig. 4 (c)) indicates the presence of strong negative coupling, i.e., a decrease in the flux with an increase in the gradient ($-\partial(q_e/n_e)/\partial\nabla T_e<0$). Thus implies negative heat diffusivity (note that the power balance heat diffusivity still satisfies $-(q_e/n_e)/\nabla T_e>0$). Negative heat diffusivity is often observed in the transition phase [21].

The non-local T_e rise takes place in the low-n_e and high-T_e (low collisionality) regime in LHD just as TFTR scaling predicts. [7, 9, 10]. There is a critical density below which the non-local transport takes place. The relationships between heat flux and temperature gradient are determined from Lissajous diagrams. The flux-gradient

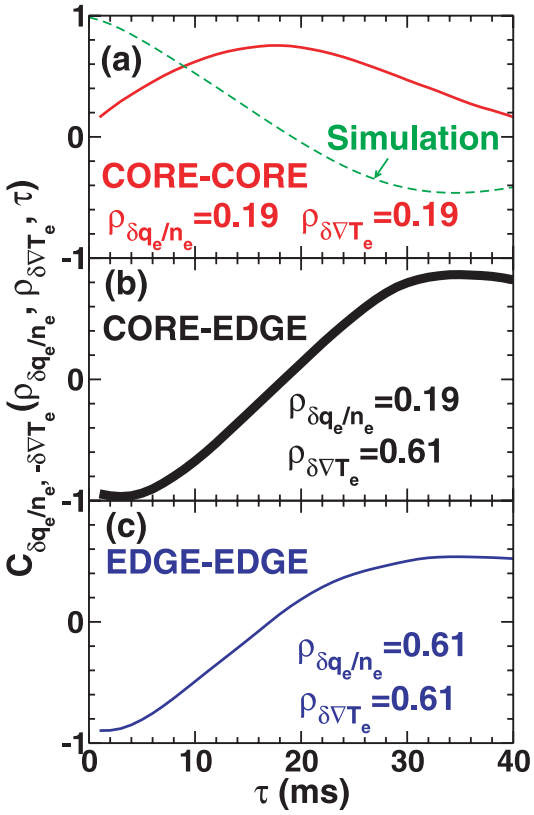

Fig. 4 Cross-correlation functions between the core heat flux and core temperature gradient ($\rho_{\delta q_e/n_e}=0.19$, $\rho_{\delta\nabla T_e}=0.19$), the core heat flux and edge temperature gradient ($\rho_{\delta q_e/n_e}=0.19$, $\rho_{\delta\nabla T_e}=0.58$), and the edge heat flux and edge temperature gradient ($\rho_{\delta q_e/n_e}=0.58$, $\rho_{\delta\nabla T_e}=0.58$). The simulated core-to-core cross correlation function is also shown in Fig. 4 (a) (green line).

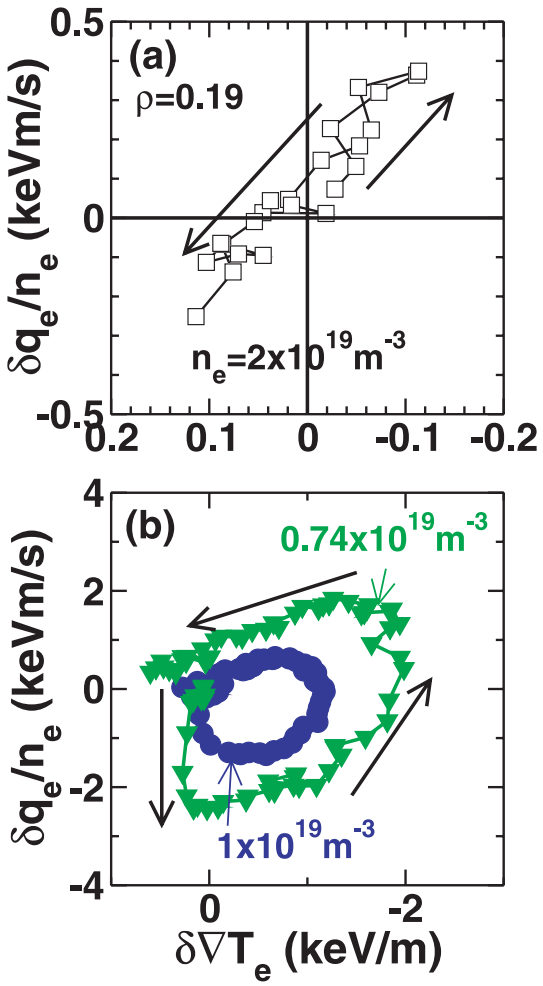

Fig. 5 Flux-gradient Lissajous diagrams at $\rho=0.19$ in (a) the local transport condition (density is above the critical value) and (b) the non-local condition (density is below the critical value). The arrows denote the direction of variation.

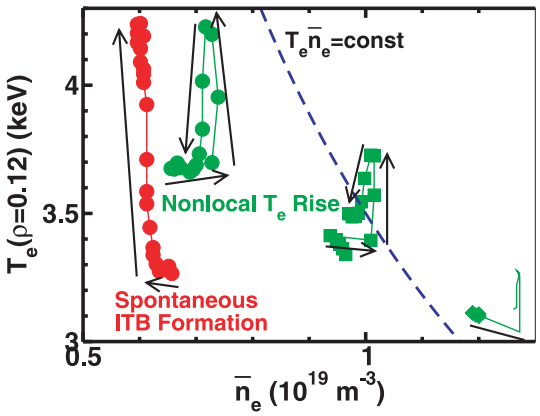

Fig. 6 Line-averaged density dependence of the change in core T_e during the non-local T_e rise and eITB formation. Arrows denote the direction of variation. The dashed line indicates a state where the core electron pressure is constant.

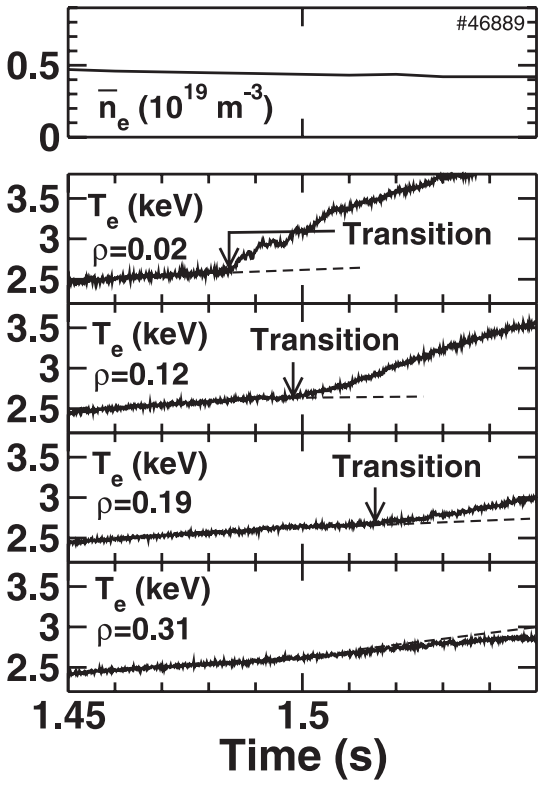

Fig. 7 Typical time evolutions of line-averaged density and T_e at different radii with spontaneous eITB formation. Arrows denote the timing of the eITB transition.

relations above and below the critical density are shown in Fig. 5. Above the critical density ($n_e = 2 \times 10^{19}$ m^{-3}), as shown in Fig. 5 (a), the obtained dynamics data lie on a straight line, and thus, the local heat flux is proportional to the local temperature gradient. On the other hand, below the critical density ($n_e = 1 \times 10^{19}$ m^{-3} and 0.74×10^{19} m^{-3}), Lissajous diagrams reveal hysteresis in heat flux versus temperature gradient. After TESPEL injection, the heat flux changes abruptly and discontinuously as shown in Fig. 5 (b). This flux jump is not accompanied by a change in the local temperature gradient, and therefore, transport is non-diffusive and non-local. The area of the hysteresis loop increases with a decrease in the density. The non-local T_e rise is considered to be one of the confinement improvements. In the confinement improvement modes, transition phenomena are frequently involved. The relationship between the heat flux and temperature gradient is responsible for transition realization. Comparison of transport dynamics in the improved mode with dynamics in the non-local T_e rise plasma is very useful to understand not only the non-local mechanisms but also the transport transient mechanisms. The responses of the core T_e to the change in the line-averaged density are shown in Fig. 6. The peak of T_e at the non-local T_e rise gradually increases with a decrease in density. The dashed line in Fig. 6 indicates a condition where the core electron pressure is constant. The peaks are, thus, not related to pressure limits. An electron internal transport barrier, eITB, is formed when collisionality becomes low enough, as shown in Fig. 6. The critical density for eITB formation is 0.6×10^{19} m^{-3} in this experiment. This value is 2-3 times smaller than that required for a non-local T_e rise (1.5×10^{19} m^{-3}). The non-local T_e rise can take place in the vicinity of the critical density for eITB formation. However, the dynamics of the non-local T_e rise and spontaneous eITB formation is quite different. Figure 7 shows the typical time evolution of T_e during spontaneous eITB formation. The eITB formation event propagates from the core to the edge and then stops near the low order rational surface ($m/n = 2/1$), as in tokamaks. The timescale of the eITB event propagation is 50 ms and is comparable to the energy confinement time of this discharge. On the other hand, propagation of the T_e rise is almost simultaneous with the non-local T_e rise [10].

3. Envelope Analysis

Interactions of turbulence over long distances are considered as a possible source for the generation of non-local coupling in plasmas. A model assuming the existence of fluctuations with long radial correlation length of the order of the minor radius has clarified several features of non-local transport dynamics [22]. However, structures with a long correlation length have not been observed previously. For further study of non-local transport, experimental observations of spatiotemporal turbulence structure are essential.

In toroidal plasmas, the most common methods to measure fluctuations are those involving density fluctuations such as conventional reflectometry. However, it is difficult to detect a certain type of fluctuation (e.g., zonal flows) by simply using density fluctuation diagnostics because the density fluctuation component is small. Recent progress in the fluctuation diagnostics (e.g., HIBP [23]) has clarified the non-linear coupling of drift wave turbulence and meso-scale structures. For example, the am-

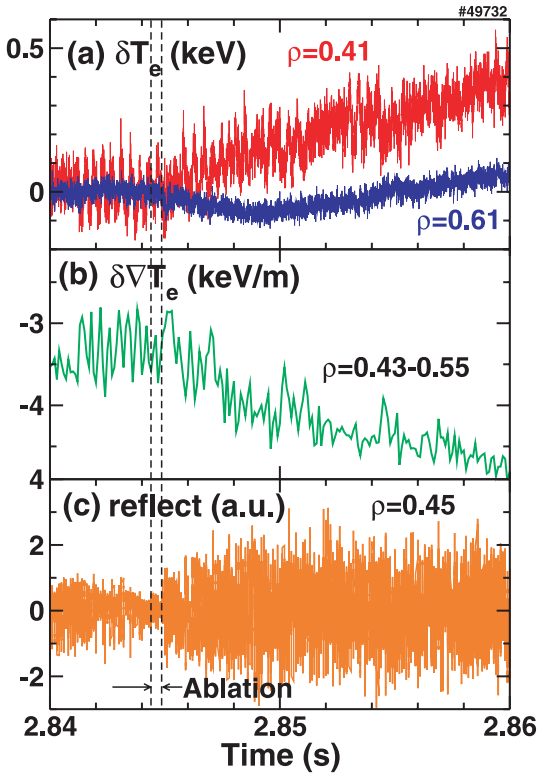

Fig. 8 Time evolution of (a) δT_e at $\rho = 0.41$ and 0.61, (b) averaged temperature gradient in the region of $\rho = 0.43-0.55$, and (c) X-mode reflectometry signal at $\rho = 0.45$.

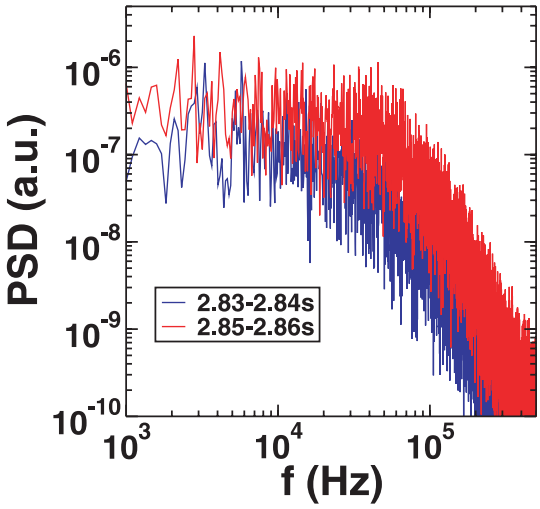

Fig. 9 Power spectral densities of the reflectometry signal at $\rho = 0.45$ before (blue line) and after (red line) TESPEL injection. Note the high pass filter ($\geq$ 1 kHz) is applied to the reflectometry signal.

plitude of turbulent density fluctuations is modulated by zonal flows through parametric modulational instability [13]. Thus, density fluctuations hold some information about the different spatial scale structures that modulate them [24]. Multi-channel reflectometry, therefore, is capable of measuring the structure correlation length (i.e., spatial scale of structure). Two channel X-mode reflectometry

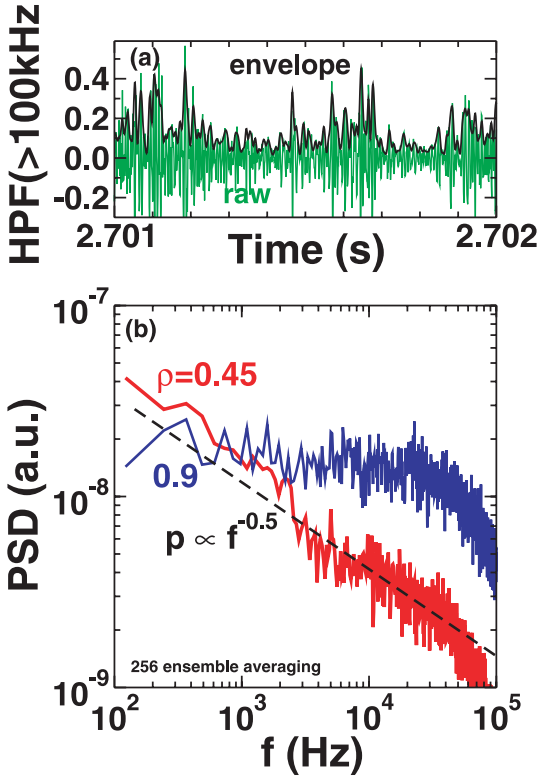

Fig. 10 (a) Time evolution of high-pass filtered signal ($\geq$ 100 kHz) at $\rho = 0.45$ and its envelope. (b) Envelope power spectrum densities at two different normalized radii.

was employed on low density plasma in LHD. Figure 8 shows the typical time evolution of a reflectometry signal during the non-local T_e rise. After a TESPEL injection, T_e at $\rho = 0.61$ drops and T_e at $\rho = 0.41$ rises, and hence, the temperature gradient begins to increase. The reflectometry signal ($\geq$ 10 kHz) at $\rho = 0.45$ increases after TESPEL injection as shown in Fig. 9. This enhancement of density fluctuation may be driven by an increase in the pressure gradient at $\rho = 0.45$. In order to deduce the existence of a modulator, envelope analysis is performed. We consider the reflectometry signal in the high frequency band ($\geq$ 100 kHz) to be an index of turbulent density fluctuation. Figure 10 shows an example of the turbulent component, its envelope, and the envelope power spectrum densities. An envelope (black line in Fig. 10 (a)) is calculated from a high-pass filtered signal ($\geq$ 100 kHz) using a Hilbert transform. The reflectometry signal data in stationary state before TESPEL injection are used for ensemble averaging to reduce statistical error. It is found that the envelope is modulated. The power spectrum density at $\rho = 0.45$ is strong in the low frequency region ($\leq$ 2 kHz). In other words, some sort of structure exists that can modulate the amplitude of the micro turbulent fluctuations. The geodesic acoustic mode (GAM) frequency is higher ($\sim$ 10 kHz) than that of the modulator, and thus, GAM is ruled out as a candidate for the modulator. There is no significant MHD mode observed with the magnetic measurement system. The power

spectrum of the modulator may be similar to that of zonal flows [23]. In theoretical works, fluctuation of the long wavelength mode excited by background micro fluctuation is predicted as the candidate for the modulator [25]. The observed modulator is considered to have the potential to cause a long distance correlation of heat transport in LHD. To determine the spatial scale of the modulator, two-point correlation of the envelopes is required. The low frequency component is also shown in the power spectrum density of the envelope at $\rho = 0.9$ (blue line in Fig. 10 (b)). The cross-coherence of these low frequency components at different radii is approximately 0.3 (significance level of 0.004), and thus, the modulator may have a radial correlation length much longer than that of the meso-scale structures (e.g., 3 cm for zonal flows). The core heat flux is correlated to the edge temperature gradient around $\rho = 0.6$; thus, reflectometry around $\rho = 0.6$ is required to discuss the spatial correlation length of an observed modulator more precisely. Multi-channel reflectometry, coherence, and bi-spectral analysis will be the object of future work.

4. Summary

In summary, we investigated the radial correlation scale of heat transport and micro- to meso-scale or macro-scale coupling of turbulent density fluctuations in LHD plasmas, where non-local transport phenomena are observed. Cold pulse experiments were performed in LHD and they showed the existence of two types of non-local transport phenomena, i.e., the fast propagation of a cold pulse and the non-local T_e rise in the helical device, as well as in tokamaks. Simulation results indicate that the timescales of non-local transport phenomena are much shorter than the local diffusion time. The radial correlation scale of heat transport is obtained by using the cross-correlation function between perturbations of heat flux and temperature gradient at different radii. An observation of a strong correlation between the core heat flux and the edge temperature gradient in the non-local T_e rise indicates that the radial correlation scale of heat transport is much longer than the micro-turbulence correlation length. Thus a long distance correlation of transport is ascertained. The envelope of density turbulence indicates the existence of an amplitude modulator with low frequency (< 2 kHz) in this plasma. The non-linear coupling of micro-turbulence with meso- or macro-structures is a possible candidate for such modulator. Interactions of turbulence over long distances are important to understand the non-local transport mechanisms. The radial length of the turbulence modulator and the radial correlation scale of transport will be compared in future work.

Acknowledgments

We thank Professor O. Motojima for his continuous encouragements. We are grateful to the technical group for their excellent support. This work is partly supported by a Grant-in-Aid for Specially Promoted Research (16002005) and by collaboration programs of NIFS (NIFS07KOAP017).

[1] H. Maassberg *et al.*, Phys. Fluids B **5**, 3627 (1993).
[2] F. Castejòn *et al.*, Nucl. Fusion **42**, 271 (2002).
[3] B. P. van Milligen *et al.*, Nucl. Fusion **42**, 787 (2002).
[4] V. V. Parail *et al.*, Nucl. Fusion **37**, 481 (1997).
[5] U. Stroth *et al.*, Plasma Phys. Control. Fusion **38**, 1087 (1996).
[6] K. W. Gentle *et al.*, Phys. Rev. Lett. **74**, 3620 (1995).
[7] M. W. Kissick *et al.*, Nucl. Fusion **38**, 821 (1998).
[8] P. Mantica *et al.*, Phys. Rev. Lett. **82**, 5048 (1999).
[9] S. Inagaki *et al.*, Plasma Phys. Control. Fusion **48**, A251 (2006).
[10] N. Tamura *et al.*, Nucl. Fusion **47**, 449 (2007).
[11] M. N. Rosenbluth and F. L. Hinton, Phys. Rev. Lett. **80**, 724 (1998).
[12] Z. Lin *et al.*, Science **281**, 1835 (1998).
[13] K. Itoh, P. H. Diamond, S.-I. Itoh and T. S. Hahm, Plasma Phys. Control. Fusion **47**, R5 (2005).
[14] M. Yagi *et al.*, Plasma Fusion Res. **2**, 0251 (2007).
[15] F. Ryter *et al.*, Phys. Rev. Lett. **86**, 5498 (2001).
[16] S. Inagaki *et al.*, Nucl. Fusion **46**, 133 (2006).
[17] O. Motojima *et al.*, Nucl. Fusion **43**, 1674 (2003).
[18] S. Sudo *et al.*, Plasma Phys. Control. Fusion **44**, 129 (2002).
[19] H. Yamada *et al.*, Nucl. Fusion **43**, 749 (2003).
[20] K. Kawahata *et al.*, Rev. Sci. Instrum. **74**, 1449 (2003).
[21] K. Ida *et al.*, Phys. Rev. Lett. **96**, 125006 (2006).
[22] T. Iwasaki *et al.*, J. Phys. Soc. Japan **68**, 478 (1999).
[23] A. Fujisawa *et al.*, Phys. Rev. Lett. **93**, 165002 (2004).
[24] Y. Nagashima *et al.*, Plasma Phys. Control. Fusion **49**, 1611 (2007).
[25] S.-I. Itoh and K. Itoh, Plasma Phys. Control. Fusion **43**, 1055 (2001).